DIFFUSIVE ELECTRON ACCELERATION AT SNR SHOCK FRONTS AND THE OBSERVED SNR RADIO SPECTRAL INDICES

T. J. Bogdan
High Altitude Observatory, National Center for Atmospheric Research
P.O. Box 3000, Boulder, CO 80307

M. A. Lee
Space Science Center, University of New Hampshire
Durham, NH 03824

I. Lerche
University of South Carolina
Columbia, SC 29208

G. M. Webb
Lunar and Planetary Laboratory, University of Arizona
Tucson, AZ 85721

1. Introduction. The radio synchrotron emission from relativistic electrons in shell supernova remnants (SNRs) provides a unique opportunity to probe the energy distribution of energetic electrons at their acceleration site (SNR shock fronts). This information provides insight into the acceleration mechanism(s). Here we discuss the implications of these observations for the diffusive (first-order Fermi) acceleration of electrons at the SNR shock fronts.

2. Observations. In Figs. 1 and 2, the diameter, D, and radio spectral index, α (defined by the relation, $S_\nu \sim \nu^\alpha$, where S_ν is the radio flux density, and ν is the observing frequency) are plotted for SNRs in our Galaxy [8, 12] and in the Large Magellanic Cloud (LMC) [14]. In Fig. 1, the filled circles and diamonds are taken from Clark and Caswell's [8] Tables I and II respectively, and the open triangles are from Göbel et al. [12]. We have omitted the 20 SNRs Weiler [16] classifies as plerions (Class P) or Class C objects, so our sample is representative of shell (Class S) SNRs. For the LMC SNRs, this distinction is not easily made. The open circles in Fig. 2 represent SNRs with optical diameters significantly in excess of their radio diameters. These objects may not be Class S objects. The uncertainties in α ($\approx \pm$ 0.05), and especially D ($\approx \pm$ 10 pc), are considerably larger than the extent of the points used in Fig. 1. Perhaps the open triangles are the most reliable galactic data since their α's are determined from at least three flux measurements (408 MHz, 1, 5 GHz), and they function as distance calibrators (via the Σ–D relation) for the filled points [5]. On the other hand, the relative D values in Fig. 2 should be quite realistic, although their overall scaling depends upon the assumed distance to the LMC ($\approx$ 55 kpc).

As noted previously [8, 13] there is a complete lack of correlation of α with D. Rather, $\langle\alpha\rangle \approx -.5$ with a spread $\Delta\alpha \approx \pm 0.15$ in both Fig. 1 and 2. The range of estimated diameters is comparable in both plots.

3. Interpretation. There have been a number of attempts to obtain constraints on and insight into acceleration mechanisms via the data presented in Fig. 1 and 2 [6, 10, 13]. In the remainder of this paper we will attempt to interpret this data in terms of the diffusive (first-order Fermi) acceleration mechanism at the SNR shock front [1, 2, 11, 15].

In its most naive form, this theory predicts a definite relationship between α and the effective compression ratio, $\bar{r}$, which the 0.1 - 10 GeV electrons responsible for the radio emission (assuming $10^{-4} < B < 10^{-6}$ gauss) sample in their scattering across the shock front:

$\alpha = -1.5/(\bar{r}-1)$. Now the gyro-radii of these same electrons are certainly $<10^{-6}D$, so it is plausible that the spatial extent of the scattering centers about the subshock (e.g. the region where the flow velocity decreases continuously from its upstream to its downstream value) reduces $\bar{r}$ from the net compression through the entire shock, r [4, 15]. If the electron scattering mean free path increases rapidly with a characteristic length that is comparable to the spatial extent of the subshock, and is a monotone increasing function of the electron momentum, then the shock-accelerated electron energy spectrum need not even exhibit a power-law behavior [15]. The spatial extent of the subshock and the scattering zone need not, however, be equal (though they may be weakly correlated), in which case $\bar{r}$ is simply the compression across the scattering zone and not r [4]. While r is likely to correlate with D, [2,7] $\bar{r}$, which is determined by the spatial character of the turbulence and hydromagnetic waves generated by the shock, must be rather sensitive to the detailed nature of the surrounding interstellar medium (ISM) (e.g., the strength, orientation and fluctuations in the galactic magnetic field; the clumpiness of a multicomponenet ISM, etc.). Thus a distribution of α's below some upper bound $-1.5/(r-1)$ may result from the variations in the position and extent of the scattering zone relative to the subshock from SNR to SNR. This would suggest that the SNRs in Figs. 1 and 2 should lie to the right of some bounding curve, say $\alpha = \alpha_c(D)$, that is itself less sensitive to the detailed structure of the ISM, but related more to the average properties of the ISM, and the energy release in the initial SNR explosion.

The net compression r must also depend upon the radiative/conductive cooling flux $\dot{Q}$ [10, 13]. Cooling fluxes [3, 7] on the order of $\approx uP$ (u-shock velocity, P-post shock pressure) are required to produce the observed spectral indices as flat as -0.25 in a $\gamma = 5/3$ gas. Certainly the conductive flux will be influenced by the local structure of the magnetic field in the ISM, as well as the presence of dense clouds [9], and may well vary significantly from SNR to SNR. If the bounding curve $\alpha = \alpha_c(D)$ incorporates the maximal $\dot{Q}$, then the spread in α for a given D follows naturally in terms of variations in $\dot{Q}$ and the structure of the electron scattering zone from one SNR to the next.

4. Conclusions. While we argue (as does Drury [10]) that diffusive electron acceleration at SNR shock fronts can qualitatively account for the data in Figs. 1 and 2, this speculation does *not* address the key trend in the data: $\langle\alpha\rangle \approx -0.5$ and $\Delta\alpha \approx \pm 0.15$. Nor have we touched upon the temporal evolution of α observed in several SNRs (see e.g. [2]), and the implications this may have for the acceleration mechanism. It is clear, however, that the similarities between Figs. 1 and 2 give us an important clue as to the ultimate source of energetic particles and perhaps, indirectly, the nature of the ISM.

Quantitative progress hinges upon a study of the self-consistent evolution of the hydromagnetic wave intensity and particle distibution across a shock with structure. If such a program can be carried out, then via $\langle\alpha\rangle$, $\Delta\alpha$ and the location of the $\alpha_c(D)$ boundary, the radio SNRs may eventually become a most valuable probe of the detailed nature of the ISM in our Galaxy and perhaps other galaxies as well.

Acknowledgments. The National Center for Atmospheric Research is sponsored by the National Science Foundation.

References.

1. Axford, W. I., E. Leer, and G. Skadron, (1977), *Proc. 15th ICRC,* **11,** 132.
2. Beck, R., L. O'C., Drury, H. J. Völk, and T. J. Bogdan, (1985), *Proc. 19th ICRC,* OG 8.1-10.
3. Blandford, R. D. and L. L. Cowie, (1982), *Ap. J.,* **260,** 625.
4. Bogdan, T. J. and I. Lerche, (1985), *MNRAS,* **212,** 413.
5. Caswell, J. L. and I. Lerche, (1979), *MNRAS,* **187,** 201.

6. Caswell, J. L. and I. Lerche, (1979), *Proc. ASA,* **3,** (5), 343.
7. Chevalier, R. A., (1977), *Ann. Rev. Astr. Ap.,* **15,** 175.
8. Clark, D. H. and J. L. Caswell, (1976), *MNRAS,* **174,** 267.
9. Cowie, L. L. and C. F. McKee, (1977), *Ap. J.,* **211,** 135.
10. Drury, L. O'C., (1983), *Sp. Sci. Rev.,* **36,** 57.
11. Drury, L. O'C., (1983), *Rep. Prog. Phys.,* **46,** 973.
12. Göbel, W., W. Hirth, and E. Fürst, (1981), *Astr. Ap,* **93,** 43.
13. Lerche, I., (1980), *Astr. Ap.,* **85,** 141.
14. Mills, B. Y., A.J. Turtle, A.G. Little, and J.M. Durdin, (1984), *Aust. J. Phys.,* **37,** 321.
15. Webb, G. M., T. J. Bogdan, M. A. Lee, and I. Lerche, (1985), *MNRAS,* (in press).
16. Weiler, K. W., (1983), in *Supernova Remnants and Their X-Ray Emission,* ed.: J. Danziger and P. Gorenstein, (Dordrecht: Reidel), p. 299.

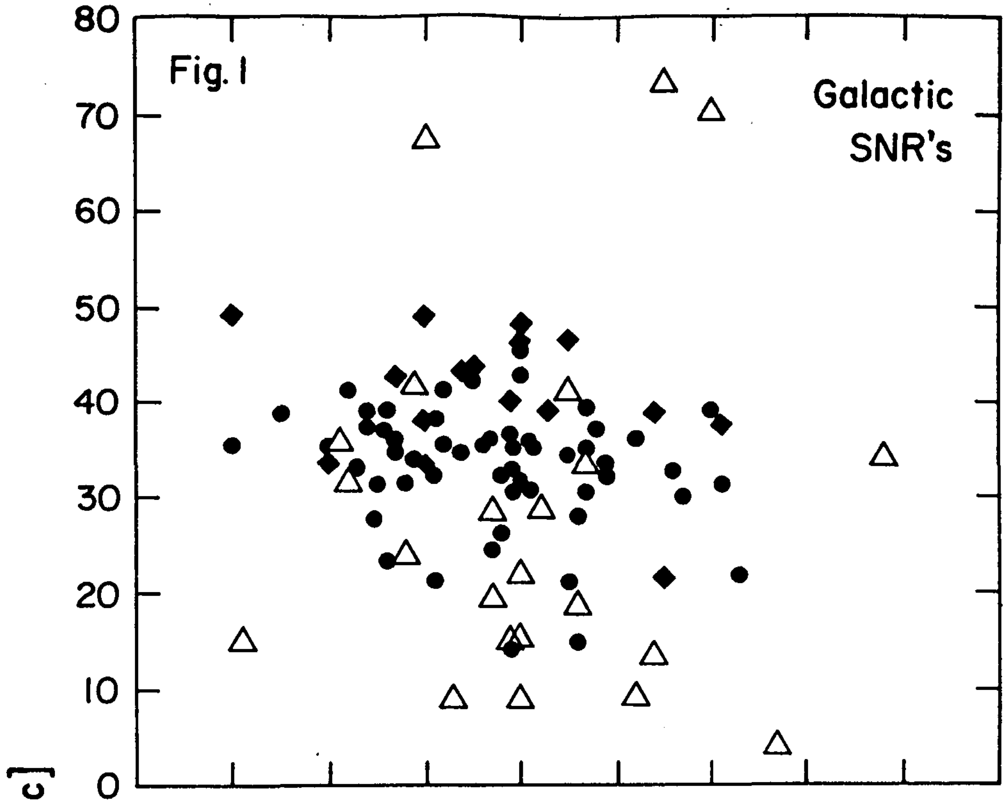
Fig. 1
Galactic SNR's
D [pc]
80
70
60
50
40
30
20
10
0

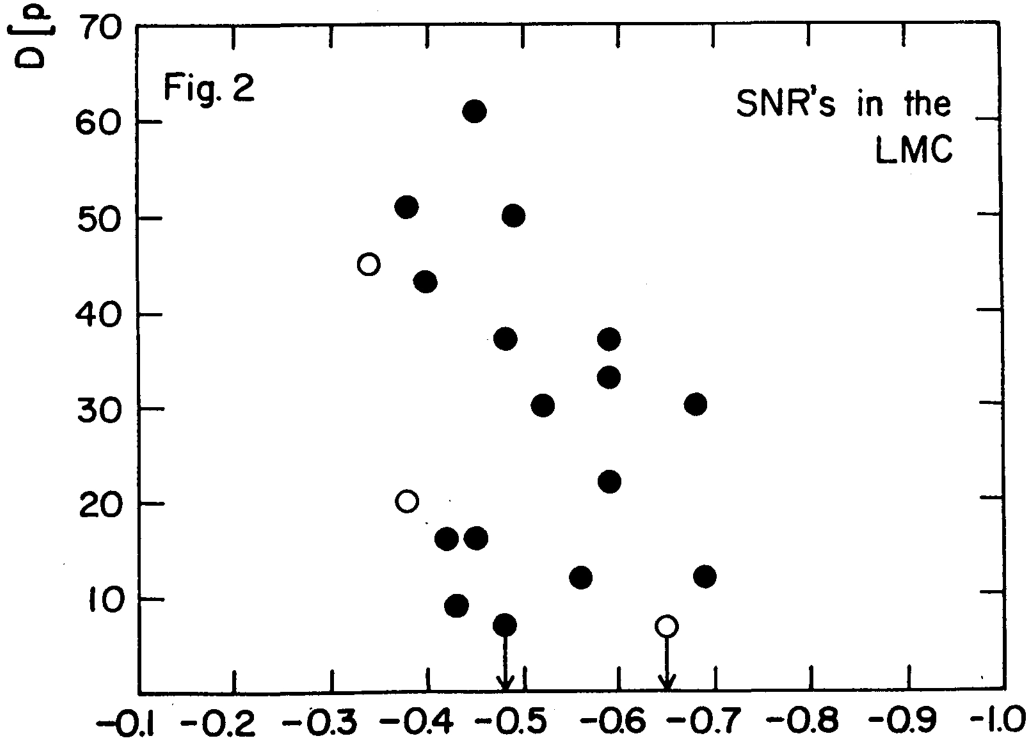
Fig. 2
SNR's in the LMC
70
60
50
40
30
20
10
-0.1
-0.2
-0.3
-0.4
-0.5
-0.6
-0.7
-0.8
-0.9
-1.0